

Quantum gas microscopy of an attractive Fermi-Hubbard system

Debayan Mitra, Peter T. Brown, Elmer Guardado-Sanchez, Stanimir S. Kondov, Trithep Devakul, David A. Huse, Peter Schauß and Waseem S. Bakr*

The attractive Fermi-Hubbard model is the simplest theoretical model for studying pairing and superconductivity of fermions on a lattice. It exhibits many interesting features including a short-coherence length at intermediate coupling and a pseudogap regime with anomalous properties. Here we study an experimental realization of this model using a two-dimensional (2D) atomic Fermi gas in an optical lattice. Using a new technique for selective imaging of doublons with a quantum gas microscope, we observe chequerboard doublon density correlations in the normal state close to half-filling. With the aid of quantum Monte Carlo simulations, we show that the measured doublon density correlations allow us to put a lower bound on the strength of s-wave pairing correlations in our system. We compare the temperature sensitivity of the doublon density correlations and the paired atom fraction and find the correlations to be a much better thermometer. Accurate thermometry of attractive lattice systems will be essential in the quest for optimizing cooling schemes to reach superfluid phases in future experiments.

he Fermi–Hubbard model is a fundamental condensed matter model for studying strongly correlated fermions on a lattice¹⁻³. With attractive interactions, it has been a fruitful theoretical playground for exploring the crossover from Bose–Einstein condensation (BEC) of local pairs to Bardeen–Cooper–Schrieffer (BCS) superconductivity in a lattice setting^{2,4,5}. Unlike its repulsive counterpart, the spin-balanced attractive model is not plagued by the fermion 'sign problem'. This has historically made it of immense pedagogical value in exploring short-coherence length superconductivity and pseudogap phenomena of the kind observed in the cuprates, despite the fact that it is now known that it is not a correct microscopic description of these materials⁵⁻⁸.

In recent years, there has been much interest in quantum simulations of the Hubbard model using cold atoms in optical lattices. In contrast to the case of repulsive interactions^{9–18}, the attractive model has received much less attention from the cold atom community^{19–21}. In the continuum, strongly interacting attractive fermions have been studied using Feshbach resonances, resulting in the observation of superfluid gases across the BEC–BCS crossover²². Fermionic superfluids have also been prepared in optical lattices close to a Feshbach resonance²³. However, these systems are not described by a simple Hubbard model due to multi-band couplings and off-site interactions^{24–27}.

In this work, we focus on the 2D attractive Fermi–Hubbard model which has been theoretically studied in detail^{2,4,28–30}. Our experiments are performed at an interaction energy small compared to the bandgap, where the single-band Hubbard description is applicable. In a grand-canonical ensemble, the Hamiltonian of the system is given by $\mathcal{H} = -t \sum_{\langle \mathbf{rr}' \rangle, \sigma} (c_{\mathbf{r}, \sigma}^\dagger c_{\mathbf{r}', \sigma} + c_{\mathbf{r}', \sigma}^\dagger c_{\mathbf{r}, \sigma}) + U \sum_{\mathbf{r}} n_{\mathbf{r}, \uparrow} n_{\mathbf{r}, \downarrow} - \mu \sum_{\mathbf{r}, \sigma} n_{\mathbf{r}, \sigma}$. Here $c_{\mathbf{r}, \sigma}^\dagger$ is the creation operator for a fermion with spin σ on site \mathbf{r} , $n_{\mathbf{r}, \sigma} = c_{\mathbf{r}, \sigma}^\dagger c_{\mathbf{r}, \sigma}$, t is the tunnelling matrix element between nearest-neighbour lattice sites, U < 0 is the strength of the on-site interaction and μ is a spin-independent chemical potential. At low temperatures, the fermions undergo a Berezinskii–Kosterlitz–Thouless (BKT) transition to a superfluid phase. As U/t becomes more negative, the superfluid

crosses over from a BCS-type superfluid to a BEC of hardcore bosons, with the critical temperature reaching a maximum in the intermediate coupling regime. Near this maximum and in the BEC regime, numerical calculations indicate a clear separation between a temperature scale T^* at which fermions start to pair and the BKT transition temperature $T_{\rm c}$ (ref. 4).

As the temperature of the system is reduced towards and below T_c , it is theoretically predicted that the fermions should exhibit charge-density-wave and pairing correlations^{4,28}. These two kinds of correlations in the system can be understood as antiferromagnetic correlations of different projections of a pseudo-spin defined on each site³¹. Formally, rotations of the pseudo-spin on site $\mathbf{r} = (r_x, r_y)$ are generated by the charge-density fluctuation operator $\eta_{\rm r}^z = (n_{\rm r} - 1)/2$ and the pairing operators $\eta_{\rm r}^- = (-1)^{r_x + r_y} c_{{\rm r},\uparrow} c_{{\rm r},\downarrow}$ and $\eta_r^+ = (\eta_r^-)^{\dagger}$ (see Methods for more details). The local pseudo-spin vector is defined by $(\eta_r^x, \eta_r^y, \eta_r^z)$, where $\eta_r^{\pm} = \eta_r^x \pm i\eta_r^y$ and the pseudo-spin vector is aligned with (against) the z-axis for a site with a doublon (hole). Pairing (density) correlations correspond to correlations of the projection of the pseudo-spin in the xy-plane (along the z-axis). The Hubbard Hamiltonian is rotationally invariant under global pseudo-spin rotations exactly at halffilling, leading to charge-density-wave (CDW) and s-wave pairing correlations of equal strength. The SU(2) pseudo-spin symmetry drives the critical temperature to zero. Away from half-filling, the degeneracy is lifted, and pairing correlations exhibit quasi-longrange order below a non-zero BKT critical temperature while the charge-density-wave correlations remain short range (Fig. 1a).

The dependence of pseudo-spin correlations on filling in the attractive Hubbard model mirrors the dependence of spin correlations on spin imbalance in the repulsive model, a topic we experimentally investigated in earlier work¹⁶. This is due to an exact mathematical mapping between the models. A particle–hole transformation on operators of \downarrow fermions in the Hubbard Hamiltonian, $c_{\mathbf{r},\downarrow} \leftrightarrow (-1)^{r_{\mathbf{x}}+r_{\mathbf{y}}}c_{\mathbf{r},\downarrow}^{\dagger}$, changes the sign of the interaction in the Hubbard Hamiltonian and exchanges the roles of pseudo-spin and spin as well as doping and spin imbalance³².

ARTICLES

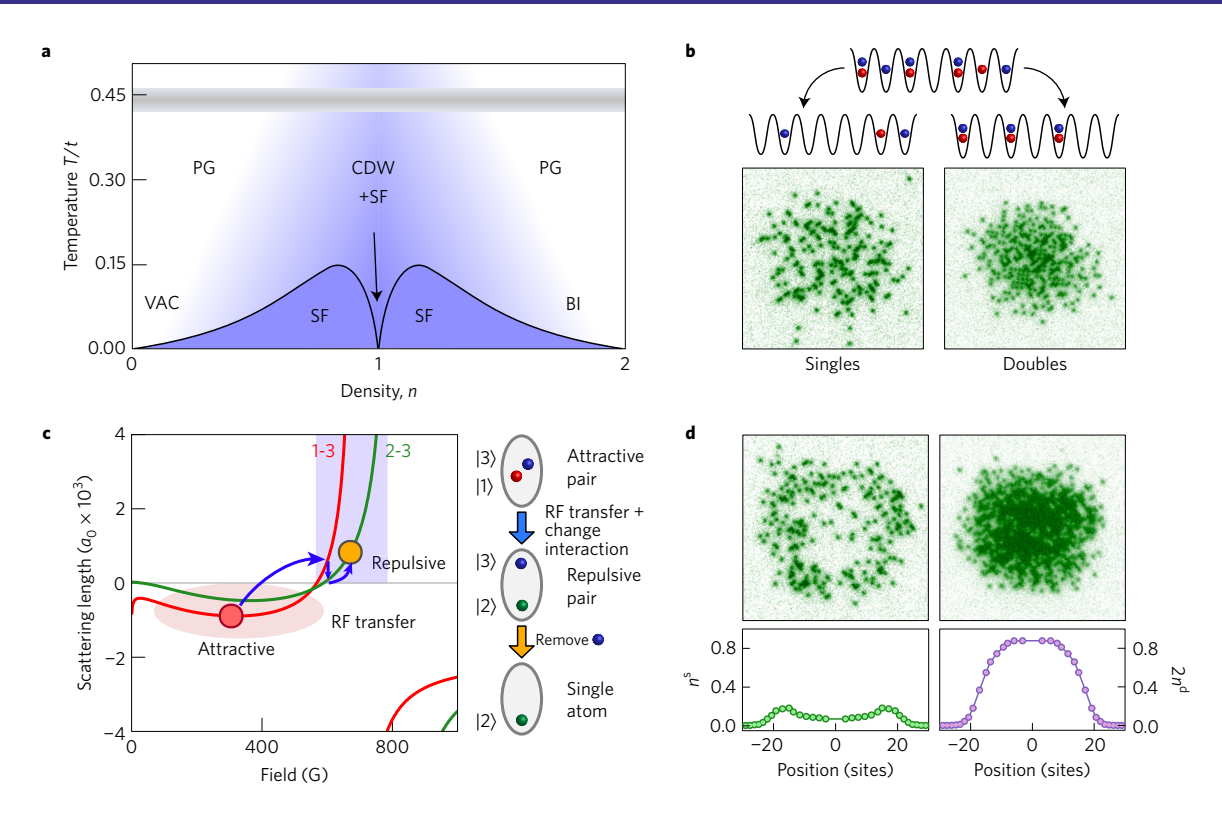


Figure 1 | **Experimental scheme for detecting densities and density correlations. a**, Schematic phase diagram of the 2D attractive Hubbard model at intermediate interaction ($U/t \approx -5$), indicating pseudogap (PG), superfluid (SF), charge-density-wave (CDW), vacuum (VAC) and band-insulating (BI) regimes. The critical temperature vanishes at n = 1. The temperatures achieved in the experiment (grey band) are above the BKT critical temperature but precursor correlations are present in the system. **b**, Single-shot fluorescence images of the singles density n^s (left) and the doublon density n^d (right). In any single image, we can either detect atoms in the singly occupied sites of the lattice only or in the doubly occupied sites only. **c**, Overview of magnetic fields and interactions used in the experimental sequence. Lines represent 6 Li scattering length versus field for a 1-3 mixture (red) and a 2-3 mixture (green) 48 . We load the lattice at attractive interactions of $a_{13} = -889a_0$ (red circle). After freezing the density distribution, we convert 1-3 doublons to 2-3 doublons, of which the state $|3\rangle$ atom is removed in a regime of repulsive interactions and we are left with only one atom per site (orange circle at $a_{23} = 414a_0$). The diagram to the right illustrates the two steps of the doublon detection: first an interaction dependent transfer and switch to repulsive interactions and then the pushing of one state of the pair which only works well at repulsive interactions. **d**, Calibration of the efficiency of the scheme to detect doublons in single-site imaging using a band-insulating region in the centre of the trap. Top, single image of singles (left) and doublons (right). Bottom, azimuthal average of ten images of singles (left) and doubles (right). In the centre, single occupancy is largely suppressed, while the double occupancy exhibits a plateau. Lines are atomic limit fits to the density profiles.

In this work, we perform a site-resolved study of the attractive Hubbard model with a fermionic quantum gas microscope ^{16,33–38} at temperatures above the BKT transition temperature. We measure the in-trap distributions of single and double occupancies and observe doublon density correlations for different fillings. Because the gas is mostly composed of on-site pairs, the doublon density, like the total density, exhibits chequerboard correlations. This observation allows us to put a lower bound on pairing correlations in the system. Furthermore, the measured correlations enable us to perform accurate thermometry on the attractive lattice gas at the superexchange scale. Thermometry at this scale is important for future work aimed at observing lattice superfluid phases, including homogeneous superfluids in spin-balanced gases and Fulde–Ferrell–Larkin–Ovchinnikov (FFLO) superfluids in spin-imbalanced gases^{39,40}.

We realize the 2D Fermi–Hubbard model using a degenerate mixture of two hyperfine ground states, $|\uparrow\rangle\equiv|1\rangle$ and $|\downarrow\rangle\equiv|3\rangle$, of ⁶Li in an optical lattice, where $|k\rangle$ labels the kth lowest hyperfine ground state. A spin-balanced mixture is obtained by optical evaporation in the vicinity of the broad Feshbach resonance centred at 690 G. After the evaporation, the scattering length is set to $-889a_0$, where a_0 is the Bohr radius, obtained by adjusting a bias magnetic field to 305.4(1) G. The mixture is prepared in a single layer of an accordion lattice (for details see ref. 41) and subsequently

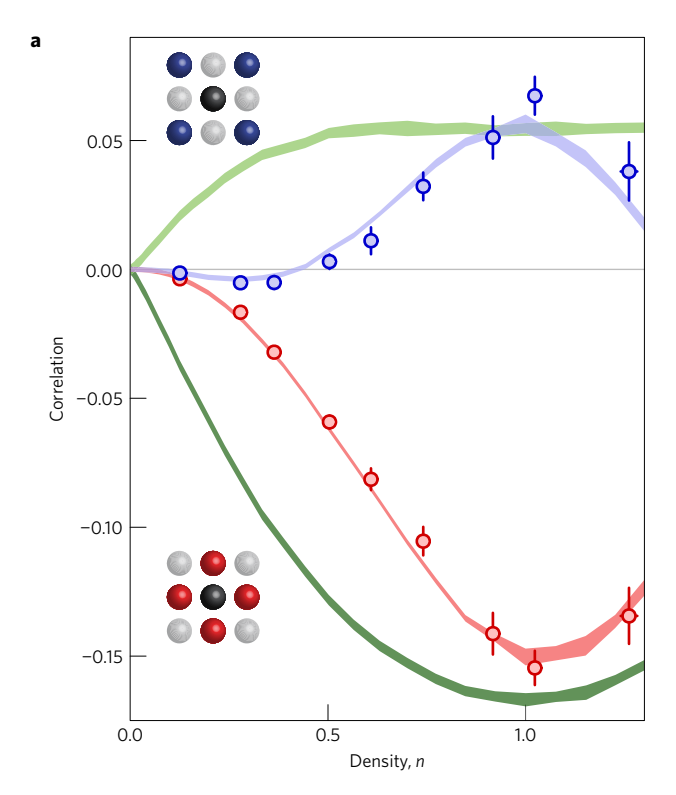
loaded adiabatically into a 2D square lattice of depth $6.2(2)E_{\rm R}$, where $t=h\times 1150(50)$ Hz. The lattice depth is chosen experimentally to maximize the observed doublon density correlations at half-filling (see Methods). Here, $E_{\rm R}=(\pi\hbar)^2/2ma_{\rm latt}^2=h\times 14.66\,{\rm kHz}$ is the recoil energy, where $a_{\rm latt}=1,064\,{\rm mm}/\sqrt{2}$ is the lattice constant. For these parameters, we obtain U/t=-5.4(3) from a bandstructure calculation and a spectroscopic determination of the interaction energy.

We extract the density profiles and correlations in the cloud from site-resolved fluorescence images obtained using quantum gas microscopy techniques (Fig. 1b). After freezing the density distribution in a deep lattice, we shine near-resonant light on the atoms in a Raman-cooling configuration. Light-assisted collisions eliminate atoms on doubly occupied sites, and we measure the singles density $n^s = n_{\uparrow} + n_{\downarrow} - 2n_{\uparrow}n_{\downarrow}$. To gain the full density information, one needs to measure the doubly occupied sites as well. But they are not directly accessible, so we developed a procedure to selectively image doubly occupied sites (Fig. 1c). After freezing the dynamics, we tag doubly occupied sites using a radiofrequency (RF) pulse to transfer atoms in state $|1\rangle$ to state $|2\rangle$ only on these sites, relying on the interaction energy for spectroscopic addressing^{9,17}. We then push atoms in states $|1\rangle$ and $|3\rangle$ out of the lattice with a resonant light pulse in the presence of a repulsive interaction. Since we have a relatively weak vertical confinement, the atoms feel a cigar-shaped on-site potential. Consequently the atoms can separate in the direction perpendicular to the 2D lattice plane, leading to a strong suppression of loss of state $|2\rangle$ atoms during the resonant light pulse due to light-assisted collisions. This procedure gives us access to the doublon density $n^{\rm d}=n_\uparrow n_\downarrow$. We have measured our doublon detection efficiency to be 0.91(1) by analysing the imaging fidelity of band-insulating regions in the cloud (Fig. 1d, see Methods). The average singles and doubles density profiles obtained from clouds prepared under identical conditions allow us to extract the total density profile $n=n^s+2n^{\rm d}$. For most of our measurements, we adjust the atom number to obtain a total mean density slightly above n=1 at the centre of the trap to obtain a large region in the cloud near half-filling.

Spatial correlations of the z-component of the pseudo-spin near half-filling correspond to CDW correlations, characterized by $\langle \eta_{\mathbf{r}}^z \eta_{\mathbf{r}+\mathbf{a}}^z \rangle_c = \langle \eta_{\mathbf{r}}^z \eta_{\mathbf{r}+\mathbf{a}}^z \rangle^{-1} \langle \eta_{\mathbf{r}}^z \rangle \langle \eta_{\mathbf{r}+\mathbf{a}}^z \rangle = \langle n_{\mathbf{r}} n_{\mathbf{r}+\mathbf{a}} \rangle_c / 4 = C^n(\mathbf{a}) / 4$ where \mathbf{a} is the displacement vector between two lattice sites. As the correlator of the total density is not directly accessible from our data we extract a closely related quantity, the doublon density correlator $C^{\rm d}(\mathbf{a}) = 4\langle n_{\rm r}^{\rm d} n_{\rm r+a}^{\rm d} \rangle_c$. In a gas consisting mostly of on-site pairs such as the ones discussed here, $C^{d}(\mathbf{a}) \approx C^{n}(\mathbf{a})$, and also exhibits chequerboard order (see Supplementary Fig. 6). As the attractive gas is compressible for any filling below unit filling, the local density varies across the harmonic trap. Figure 2a shows the doublon density correlator versus density for the nearestneighbour and the next-nearest-neighbour, obtained by azimuthally averaging the correlations over the trap. The corresponding trap density profile of the gas is depicted in Fig. 2b. The nearestneighbour doublon density correlator measured at half-filling, where the correlations are largest, is $C^{d}(1, 0) = -0.155(6)$. An interesting feature of the next-nearest-neighbour correlator $C^{d}(1, 1)$ is that it becomes negative as the average density falls below \sim 0.4. This can be understood in the limit of large negative U, where the system can be treated as a gas of hardcore bosons with repulsive nearest-neighbour interactions, leading to negative correlations at distances less than the interparticle spacing. In a recent experiment, we have observed similar behaviour in the next-nearest-neighbour antiferromagnetic correlations of the z-projection of the spin in a spin-imbalanced repulsive Hubbard model¹⁶. This is a consequence of the aforementioned mathematical mapping between the attractive and repulsive models.

We theoretically model our system using determinantal Quantum Monte Carlo (DQMC)⁴² in a local density approximation (LDA) and see very good agreement between theory and experiment for the doublon density correlators and density (Fig. 2 and Methods). The fits give U/t = -5.7(2) and T/t = 0.45(3). The measured temperature is comparable to our recent measurements in a repulsive gas¹⁶. We have also compared to DQMC in the presence of a spatially varying potential to reproduce the largest experimentally observed density gradients to verify that the LDA holds in our system. The fact that the same temperature fits both the doublon density correlator and the density confirms that the system is in thermal equilibrium. In addition, we have obtained the pairing correlations $C^{\Delta}(\mathbf{a})$ from DQMC. Here $C^{\Delta}(\mathbf{a}) = \langle \Delta_{\mathbf{r}}^{x} \Delta_{\mathbf{r}+\mathbf{a}}^{x} \rangle_{c}$ and the s-wave pairing operator on site **r** is defined by $\Delta_{\bf r}^x = c_{{\bf r},\uparrow}c_{{\bf r},\downarrow} + c_{{\bf r},\downarrow}^{\dagger}c_{{\bf r},\uparrow}^{\dagger}$. We find that $|C^{d}(\mathbf{a})| \leq |C^{\Delta}(\mathbf{a})|$ for any temperature, interaction strength, filling and distance between the sites (see Methods and Supplementary Fig. 2). As an example, we show the predicted pairing correlations versus density for the parameters of Fig. 2. Thus our measured doublon density correlations provide a bound on *s*-wave pairing correlations in a cold atom lattice system.

Single-site imaging of doublons allows us to also measure longer range correlations (Fig. 3). We see doublon density correlations up to two sites on a diagonal shown in the correlation matrices $C^d(i,j)$. We find good agreement with DQMC calculations corresponding to the experimental fillings, calculated using the same parameters as



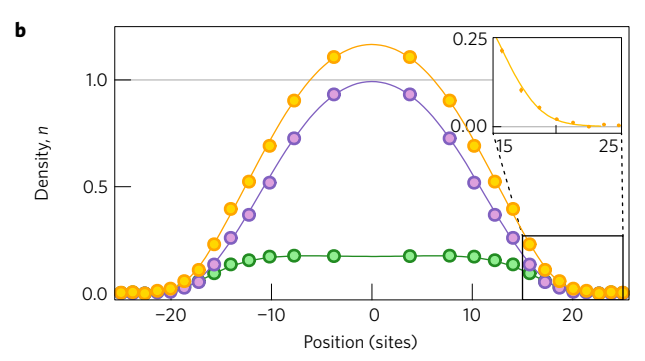


Figure 2 | **Observation of doublon density correlations. a**, Measured nearest-neighbour doublon density correlator $C^d(1,0)$ (red circles) and next-nearest-neighbour correlator $C^d(1,1)$ (blue circles) from an average of 60 repetitions. Error bars s.e.m. DQMC results for $C^d(1,0)$ (red), $C^d(1,1)$ (blue), $-C^{\Delta}(1,0)$ (dark green) and $C^{\Delta}(1,1)$ (light green) at U/t=-5.7 and T/t=0.45 are shown for comparison (bands are s.e.m. of the numerics). **b**, Density profiles. Density of singles (n^s , green circles), density of doubles ($2n^d$, purple circles) and total density ($n=n^s+2n^d$, orange circles). Lines are a simultaneous local density approximation fit of DQMC data to the total and singles densities. Inset, zoom in on the tail of the density distribution. For this fit, we fix U/t and T/t at the values above and we obtain from the fit the central chemical potential $\mu(0)=0.46(2)U<0$ and the trap frequency $\omega=2\pi\times202(5)$ Hz, in agreement with independent measurements of ω (Supplementary Information).

above. The range of the correlation becomes maximal at half-filling, as expected from theory.

Both the doublon fraction and doublon density correlations may be used as thermometers in an attractive Hubbard system. To investigate their sensitivity as thermometers, we heated the system in a controlled fashion by holding it for variable times in the lattice before imaging. Technical noise leads to a linear increase in the temperature. We observe a slight reduction in doublon fraction in a region of half-filling for long hold times (Fig. 4a), while the doublon density correlators $C^d(1,0)$ and $C^d(1,1)$ show

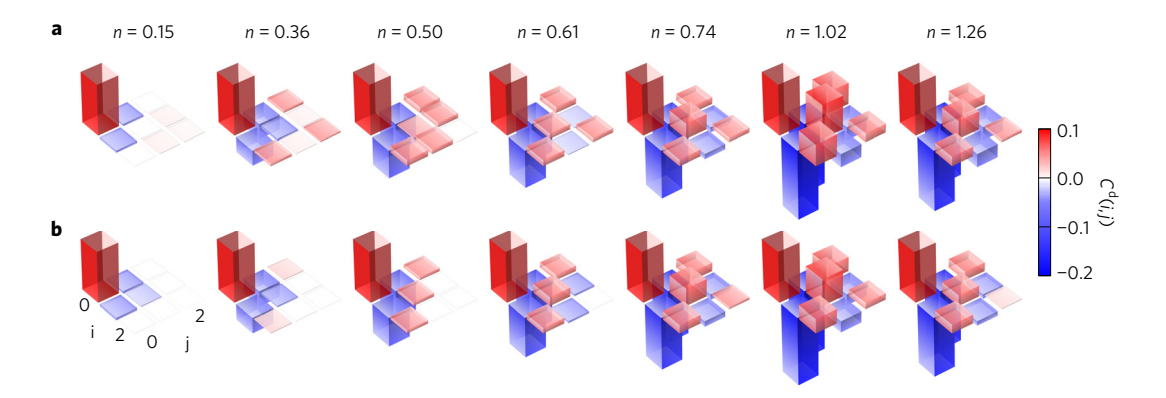


Figure 3 | **Doublon density correlation matrices for varying density. a**, Doublon density correlator $C^d(i,j)$ for average densities ranging from 0.15 to 1.26. Correlator values are averaged over 60 pictures. **b**, DQMC matrices calculated for the same parameters as in Fig. 2.

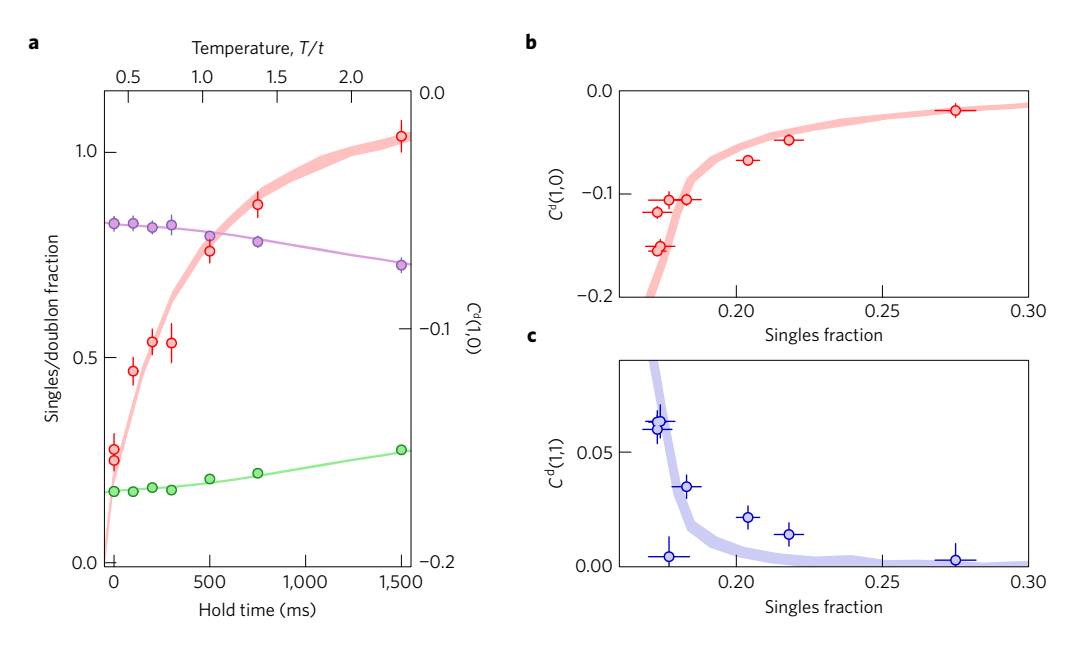


Figure 4 | Thermometry of an attractive Hubbard system. a, Temperature dependence of the paired fraction and nearest-neighbour doublon density correlations. Shown are the fraction of singles (green circles) and doubles (purple circles) at half-filling on the left axis as a function of hold time in the lattice. On the right axis is the doublon density correlator $C^d(1,0)$ (red circles) at half-filling measured for the same hold times. The upper x-axis are temperatures obtained from comparison to DQMC, giving a linear heating rate of 1.3(1) t/s. **b**, $C^d(1,0)$ as a function of singles fraction. Each data point corresponds to a single hold time. **c**, The next-nearest-neighbour doublon density correlator $C^d(1,1)$ as function of singles fraction. Bands correspond to DQMC results for U/t = -5.7 and half-filling in all of the above. Each point is averaged over 60 pictures. Error bars and bands are s.e.m.

a significant change during the same time. These observations illustrate that the doublon fraction is a good thermometer for temperatures on the order of U, where doublon density correlations are small, while the latter are more sensitive thermometer for temperatures on the order of the exchange $4t^2/U$. This is similar to the repulsive case, where spin correlations have been found to be a more sensitive thermometer than density¹⁸. Figure 4b,c shows the nearest-neighbour and next-nearest-neighbour doublon density correlators versus the singles fraction at half-filling. Plotting the data this way allows a temperature-independent comparison to DQMC with a single free parameter (U/t), and we obtain good agreement for U/t = -5.7.

In conclusion, we have performed quantum gas microscopy on an attractive atomic Fermi–Hubbard system. We have observed doublon density correlations and studied their dependence on the lattice filling and temperature, finding excellent agreement with DQMC calculations. These correlations serve as an excellent thermometer in the low-temperature regime that will help in the development of cooling schemes required for achieving long-range

Hubbard superfluids. Above the critical temperature, attractive Hubbard systems will allow experimental exploration of the physics of the pseudogap regime, while at lower temperatures, they will enable studies of the BKT transition in a lattice system. The pairing correlations inferred in this experiment may be probed more directly using collective excitations of the pairing order parameter that couple to the conjugate CDW order parameter⁴³. Another interesting direction for future work is the study of the spin-imbalanced attractive Hubbard model in 2D, where Fermi surface nesting due to the lattice increases the stability of FFLO superfluids⁴⁴⁻⁴⁷. Unlike spin-balanced gases investigated in this work, DQMC suffers a fermion 'sign problem' in simulating the spin-imbalanced attractive Hubbard model, making theoretical predictions difficult at low temperatures.

Methods

Methods, including statements of data availability and any associated accession codes and references, are available in the online version of this paper.

NATURE PHYSICS DOI: 10.1038/NPHYS4297 ARTICLES

Received 4 May 2017; accepted 19 September 2017; published online 23 October 2017

References

- 1. Hubbard, J. Electron correlations in narrow energy bands. *Proc. R. Soc. Lond. A* **276**, 238–257 (1963).
- Micnas, R., Ranninger, J. & Robaszkiewicz, S. Superconductivity in narrow-band systems with local nonretarded attractive interactions. *Rev. Mod. Phys.* 62, 113–171 (1990).
- 3. Auerbach, A. Interacting Electrons and Quantum Magnetism (Springer, 1994).
- Scalettar, R. T. et al. Phase diagram of the two-dimensional negative-U
 Hubbard model. Phys. Rev. Lett. 62, 1407–1410 (1989).
- Singer, J. M., Pedersen, M. H., Schneider, T., Beck, H. & Matuttis, H.-G. From BCS-like superconductivity to condensation of local pairs: a numerical study of the attractive Hubbard model. *Phys. Rev. B* 54, 1286–1301 (1996).
- Randeria, M., Trivedi, N., Moreo, A. & Scalettar, R. T. Pairing and spin gap in the normal state of short coherence length superconductors. *Phys. Rev. Lett.* 69, 2001–2004 (1992).
- Trivedi, N. & Randeria, M. Deviations from Fermi-liquid behavior above T_c in 2D short coherence length superconductors. *Phys. Rev. Lett.* 75, 312–315 (1995).
- Kyung, B., Allen, S. & Tremblay, A.-M. S. Pairing fluctuations and pseudogaps in the attractive Hubbard model. *Phys. Rev. B* 64, 075116 (2001).
- Jördens, R., Strohmaier, N., Günter, K., Moritz, H. & Esslinger, T. A Mott insulator of fermionic atoms in an optical lattice. *Nature* 455, 204–207 (2008).
- 10. Schneider, U. et al. Metallic and insulating phases of repulsively interacting fermions in a 3D optical lattice. Science 322, 1520–1525 (2008).
- Greif, D., Uehlinger, T., Jotzu, G., Tarruell, L. & Esslinger, T. Short-range quantum magnetism of ultracold fermions in an optical lattice. *Science* 340, 1307–1310 (2013).
- 12. Hart, R. A. *et al.* Observation of antiferromagnetic correlations in the Hubbard model with ultracold atoms. *Nature* **519**, 211–214 (2015).
- 13. Parsons, M. F. *et al.* Site-resolved measurement of the spin-correlation function in the Fermi-Hubbard model. *Science* **353**, 1253–1256 (2016).
- Cheuk, L. W. et al. Observation of spatial charge and spin correlations in the 2D Fermi-Hubbard model. Science 353, 1260–1264 (2016).
- Boll, M. et al. Spin- and density-resolved microscopy of antiferromagnetic correlations in Fermi-Hubbard chains. Science 353, 1257–1260 (2016).
- Brown, P. T. et al. Spin-imbalance in a 2D Fermi-Hubbard system. Science 357, 1385–1388 (2017).
- Cocchi, E. et al. Equation of state of the two-dimensional Hubbard model. Phys. Rev. Lett. 116, 175301 (2016).
- Drewes, J. H. et al. Antiferromagnetic correlations in two-dimensional fermionic Mott-insulating and metallic phases. Phys. Rev. Lett. 118, 170401 (2017).
- Strohmaier, N. et al. Interaction-controlled transport of an ultracold Fermi gas. Phys. Rev. Lett. 99, 220601 (2007).
- Hackermüller, L. et al. Anomalous expansion of attractively interacting fermionic atoms in an optical lattice. Science 327, 1621–1624 (2010).
- Schneider, U. et al. Fermionic transport and out-of-equilibrium dynamics in a homogeneous Hubbard model with ultracold atoms. Nat. Phys. 8, 213–218 (2012).
- Inguscio, M., Ketterle, W. & Salomon, C. (eds) Ultra-cold Fermi Gases, Proceedings of the International School of Physics "Enrico Fermi", Course CLXIV, Varenna 2006 922 (IOS Press, 2008).
- 23. Chin, J. K. *et al.* Evidence for superfluidity of ultracold fermions in an optical lattice. *Nature* **443**, 961–964 (2006).
- Duan, L.-M. Effective Hamiltonian for fermions in an optical lattice across a Feshbach resonance. *Phys. Rev. Lett.* 95, 243202 (2005).
- Carr, L. D. & Holland, M. J. Quantum phase transitions in the Fermi–Bose Hubbard model. *Phys. Rev. A* 72, 031604 (2005).
- Zhou, F. Mott states under the influence of fermion-boson conversion. Phys. Rev. B 72, 220501 (2005).
- Diener, R. B. & Ho, T.-L. Fermions in optical lattices swept across Feshbach resonances. *Phys. Rev. Lett.* 96, 010402 (2006).
- Hirsch, J. E. Two-dimensional Hubbard model: numerical simulation study. Phys. Rev. B 31, 4403–4419 (1985).

- Moreo, A. & Scalapino, D. J. Two-dimensional negative-U Hubbard model. Phys. Rev. Lett. 66, 946–948 (1991).
- 30. Paiva, T., dos Santos, R. R., Scalettar, R. T. & Denteneer, P. J. H. Critical temperature for the two-dimensional attractive Hubbard model. *Phys. Rev. B* **69**, 184501 (2004).
- 31. Yang, C. N. & Zhang, S. C. SO₄ symmetry in a Hubbard model. *Mod. Phys. Lett. B* $\bf 04$, 759–766 (1990).
- Ho, A. F., Cazalilla, M. A. & Giamarchi, T. Quantum simulation of the Hubbard model: the attractive route. *Phys. Rev. A* 79, 033620 (2009).
- Haller, E. et al. Single-atom imaging of fermions in a quantum-gas microscope. Nat. Phys. 11, 738–742 (2015).
- Edge, G. J. A. et al. Imaging and addressing of individual fermionic atoms in an optical lattice. Phys. Rev. A 92, 063406 (2015).
- 35. Omran, A. *et al*. Microscopic observation of Pauli blocking in degenerate fermionic lattice gases. *Phys. Rev. Lett.* **115**, 263001 (2015).
- Parsons, M. F. et al. Site-resolved imaging of fermionic ⁶Li in an optical lattice. Phys. Rev. Lett. 114, 213002 (2015).
- Cheuk, L. W. et al. Quantum-gas microscope for fermionic atoms. Phys. Rev. Lett. 114, 193001 (2015).
- Yamamoto, R., Kobayashi, J., Kuno, T., Kato, K. & Takahashi, Y. An ytterbium quantum gas microscope with narrow-line laser cooling. *New J. Phys.* 18, 023016 (2016).
- Fulde, P. & Ferrell, R. A. Superconductivity in a strong spin-exchange field. Phys. Rev. 135, A550–A563 (1964).
- Larkin, A. I. & Ovchinnikov, Yu. N. Nonuniform state of superconductors. Sov. Phys. JETP 20, 762–769 (1965).
- Mitra, D., Brown, P. T., Schauß, P., Kondov, S. S. & Bakr, W. S. Phase separation and pair condensation in a spin-imbalanced 2D Fermi gas. *Phys. Rev. Lett.* 117, 093601 (2016).
- Varney, C. N. et al. Quantum Monte Carlo study of the two-dimensional fermion Hubbard model. Phys. Rev. B 80, 075116 (2009).
- Demler, E., Zhang, S.-C., Bulut, N. & Scalapino, D. J. A class of collective excitations of the Hubbard model: η excitation of the negative-U model. *Int. J. Mod. Phys. B* 10, 2137–2166 (1996).
- Moreo, A. & Scalapino, D. J. Cold attractive spin polarized Fermi lattice gases and the doped positive *U* Hubbard model. *Phys. Rev. Lett.* 98, 216402 (2007).
- Loh, Y. L. & Trivedi, N. Detecting the elusive Larkin–Ovchinnikov modulated superfluid phases for imbalanced Fermi gases in optical lattices. *Phys. Rev. Lett.* 104, 165302 (2010).
- Kim, D.-H. & Törmä, P. Fulde–Ferrell–Larkin–Ovchinnikov state in the dimensional crossover between one- and three-dimensional lattices. *Phys. Rev.* B 85, 180508 (2012).
- Gukelberger, J., Lienert, S., Kozik, E., Pollet, L. & Troyer, M.
 Fulde–Ferrell–Larkin–Ovchinnikov pairing as leading instability on the square
 lattice. *Phys. Rev. B* 94, 075157 (2016).
- Zürn, G. et al. Precise characterization of ⁶Li Feshbach resonances using trap-sideband-resolved RF spectroscopy of weakly bound molecules. Phys. Rev. Lett. 110, 135301 (2013).

Acknowledgements

This work was supported by the NSF (grant no. DMR-1607277), the David and Lucile Packard Foundation (grant no. 2016-65128), and the AFOSR Young Investigator Research Program (grant no. FA9550-16-1-0269). W.S.B. was supported by an Alfred P. Sloan Foundation fellowship. P.T.B. was supported by the DoD through the NDSEG Fellowship Program.

Author contributions

All authors contributed extensively to the work presented in this paper.

Additional information

Supplementary information is available in the online version of the paper. Reprints and permissions information is available online at www.nature.com/reprints. Publisher's note: Springer Nature remains neutral with regard to jurisdictional claims in published maps and institutional affiliations. Correspondence and requests for materials should be addressed to W.S.B.

Competing financial interests

The authors declare no competing financial interests.

ARTICLES NATURE PHYSICS DOI: 10.1038/NPHYS4297

Methods

Preparation of an attractive Fermi gas in an optical lattice. The experimental set-up is described in detail in the supplement of ref. 16. We realize the Fermi–Hubbard model using a spin-balanced degenerate mixture of two Zeeman states ($|1\rangle = |\uparrow\rangle$ and $|3\rangle = |\downarrow\rangle$, numbered up from the lowest energy) in the ground state hyperfine manifold of ⁶Li in an optical lattice.

To create the sample we load a magneto-optical trap (MOT) from a Zeeman slower, then use a compressed MOT stage before loading into a approximately 1-mK-deep optical trap and evaporating near the 690 G Feshbach resonance. We stop the evaporation before Feshbach molecules form and transfer the atoms to a highly anisotropic 'light sheet' trap where the gas undergoes further evaporation to degeneracy at 305.4(1) G. At this field, the scattering length is $a_{\rm s}=-889a_{\rm 0}$. Next we transfer the gas into the final trapping geometry where a 1,070 nm beam provides radial confinement and a 532 nm accordion lattice with trapping frequency $\omega_z=2\pi\times21(1)$ kHz provides axial confinement (for further details see ref. 41). The spin populations are balanced to within 2.1(9)%. We then load the gas into a 2D square lattice with a 25-ms-long ramp to varying depths from $4-7.5E_r$.

Calibration of Hubbard parameters and overall confinement. We use a non-separable 2D square lattice with a 752 nm spacing formed by four interfering passes of a single vertically polarized beam ¹⁶. We calibrate our lattice depth by measuring the frequencies of the three d bands in a deep lattice using lattice depth modulation, and compare these with a 2D band structure calculation. The inferred depth of the lattice at which our measurements are performed is $6.2(2)E_r$, where $E_r = 14.66$ kHz. From that we obtain nearest-neighbour tunnelling values $t_x = 1,200$ Hz, $t_y = 1,110$ Hz ($t_x/t_y = 1.08$). The reduction of the lattice depth across the cloud due to the Gaussian profile of the lattice beams leads to an increase in the tunnelling by 10% at the edge of the cloud compared to the central value. We also calculate a non-zero but negligible diagonal tunnelling $t_{11} = 42$ Hz = $0.04t_x$, due to the non-separability of the lattice.

We measure the interaction energy U at the lattice loading field of 305 G using RF spectroscopy. We transfer atoms from state $|1\rangle$ to $|2\rangle$ and resolve the frequency shift between singly and doubly occupied sites. We determine $U_{13} = \delta U(a_{13}/(a_{13}-a_{23}))$, where δU is the measured difference between the singles and doublon peaks and a_{13} (a_{23}) is the scattering length at the spectroscopy field for a 1-3 (2-3) mixture. Taking into account this correction due to a significant final state interaction, we obtain $U_{13} = 6.6(3)$ kHz. The experimentally measured value agrees with the value determined from band structure calculations of 5.9(1) kHz including higher band corrections to within 10% (ref. 49).

The harmonic trapping potential for the attractive gas in the lattice has been checked in several independent ways. A calculation from measured beam waist and power yields 220 Hz. A spatially resolved lattice depth modulation spectroscopy allows us to extract the lattice depth variation in the radial direction, which yields 197 Hz. In addition we did a density and correlator fit to a non-interacting Fermi gas at the same lattice depth as the attractive gas, which yields 218 Hz. These values all agree within uncertainty with the value determined from the DQMC fit in the main text.

Imaging of doublons. In the usual scheme of Raman imaging, a singly occupied lattice site produces a fluorescence signal while atoms in a doubly occupied site are lost due to light-assisted collisions. To measure density correlations between doubly occupied sites, we have developed a new detection scheme. After the gas is loaded adiabatically into the optical lattice, we pin the atoms by increasing the lattice depth to $55(1)E_R$ in $100\,\mu$ s where tunnelling dynamics get frozen. The next step is to adiabatically ramp the field to $594~\rm G$ where we perform an interaction-resolved Landau–Zener sweep (Supplementary Fig. 1) to selectively transfer 1-3 doublons to 2-3 doublons while not effecting the $|1\rangle$ singles. Finally we ramp to a field of 641 G where the 2-3 scattering length is $414a_0$. We apply resonant pushing pulses of $30\,\mu$ s durations to remove $|1\rangle$ and $|3\rangle$ atoms, leaving behind only $|2\rangle$ atoms on sites that originally had doublons. The large relative wavefunction of the atoms on a site due to repulsive interactions and a relatively weak vertical confinement significantly reduces the probability of light-assisted collisions during the resonant pulse. On the other hand, to get the singles images, we apply no RF or resonant pushing pulses.

We image the final atom distribution by increasing the lattice depth to 2,500*E*, within 250 µs, ramping up the light sheet to provide axial confinement, and then collecting fluorescence photons during Raman cooling.

To measure the efficiency of imaging doublons, we prepare a band insulator where the filling in the trap centre is saturated at two atoms per site. We perform the above-mentioned process to image only the doublons. We measure a combined fidelity (including RF-transfer efficiency and pushing efficiency) of $1-\epsilon_d=91(1)\%$ of imaging doublons, leading to an underestimation of our doublon density correlator by $(1-\epsilon_d)^2=0.83$ which we correct for. We have also performed the same detection procedure on a Mott insulator, where we expect unit occupancy on the lattice sites. This allows us to extract the probability that a single atom in state $|1\rangle$ would get transferred to $|2\rangle$ and give a false positive signal of the presence of a doublon. We measure the probability of this process to be only 2.3(3)%.

Raman imaging and reconstruction. We perform Raman imaging for 1,200 ms and collect approximately 1,000 photons per atom. For more details, see ref. 16. We estimate fidelity errors due to Raman imaging imperfections by taking 40 consecutive images of the same atom cloud and determine the shot-to-shot differences. This leads to a hopping rate during one picture of 0.4(1)% and a loss rate of 1.9(2)%. In addition, while holding the atoms in a deep lattice for doublon detection, we lose 2(1)% of the atoms, leading to a net detection efficiency of approximately 95% for singly occupied sites. The densities that we obtain are corrected for the above detection efficiency.

Lower bound on pairing correlations. The full Hubbard Hamiltonian can be written as

$$\mathcal{H} = -t \sum_{\langle \mathbf{rr}' \rangle_{\sigma}} \left(c_{\mathbf{r},\sigma}^{\dagger} c_{\mathbf{r}',\sigma} + c_{\mathbf{r}',\sigma}^{\dagger} c_{\mathbf{r},\sigma} \right) + U \sum_{\mathbf{r}} n_{\mathbf{r},\uparrow} n_{\mathbf{r},\downarrow} - \mu \sum_{\mathbf{r},\sigma} n_{\mathbf{r},\sigma} - h \sum_{\mathbf{r},\sigma} \left(n_{\mathbf{r},\uparrow} - n_{\mathbf{r},\downarrow} \right)$$

$$(1)$$

where $c_{r,\sigma}^{\dagger}$ is the creation operator for a fermion with spin σ on site \mathbf{r} , $n_{t,\sigma}=c_{r,\sigma}^{\dagger}c_{t,\sigma}$, t is the matrix element for tunnelling between lattice sites, U is the strength of the on-site interaction (U<0 for the attractive model), μ is a spin-independent chemical potential and h is an effective Zeeman field in the presence of spin imbalance. For the purpose of this paper, h=0, since we work only with a spin-balanced system. Consider first the SU(2) spin symmetry of the problem for h=0. The vector spin operator on site \mathbf{r} is given by (S_r^x, S_r^y, S_r^y) , where $S_r^{\pm}=S_r^x\pm iS_r^y$. In terms of fermionic creation and annihilation operators, the generators of spin rotations are

$$S_{\mathbf{r}}^{-} = c_{\mathbf{r},\downarrow}^{\dagger} c_{\mathbf{r},\uparrow}$$

$$S_{\mathbf{r}}^{+} = (S_{\mathbf{r}}^{-})^{\dagger} = c_{\mathbf{r},\uparrow}^{\dagger} c_{\mathbf{r},\downarrow}$$

$$S_{\mathbf{r}}^{z} = \frac{1}{2} (c_{\mathbf{r},\uparrow}^{\dagger} c_{\mathbf{r},\uparrow} - c_{\mathbf{r},\downarrow}^{\dagger} c_{\mathbf{r},\downarrow}) = \frac{1}{2} (n_{\mathbf{r},\uparrow} - n_{\mathbf{r},\downarrow})$$
(2)

These operators obey the usual commutation relations

$$[S_r^z, S_r^{\pm}] = \pm S_r^{\pm}, \quad [S_r^+, S_r^-] = 2S_r^z$$
 (3)

In the absence of an effective Zeeman field, the operators $S^c = \sum_r S_r^c$ and $S^{\pm} = \sum_r S_r^{\pm}$ satisfy

$$[\mathcal{H}, S^{\pm}] = [\mathcal{H}, S^z] = 0 \tag{4}$$

implying the SU(2) spin symmetry of the Hubbard model. In other words, the Hamiltonian is invariant under a global rotation of the spin degree of freedom. To demonstrate the other 'hidden' symmetry of the Hubbard model, we define a new set of generators for rotations of the 'pseudo-spin' on a site given by

 $\eta_{\mathbf{r}}^{-} = (-1)^{r_x + r_y} c_{\mathbf{r},\uparrow} c_{\mathbf{r},\downarrow}$

$$\eta_{\rm r}^+ = (\eta_{\rm r}^-)^{\dagger}$$

$$\eta_{\rm r}^z = \frac{1}{2}(n_{\rm r} - 1) \tag{5}$$

It can be easily verified 50 that they obey the following commutation relations

$$[\eta_r^z, \eta_r^{\pm}] = \pm \eta_r^{\pm}, \quad [\eta_r^+, \eta_r^-] = 2\eta_r^z$$
 (6)

The operators $\eta^z = \sum_{z} \eta_z^z$ and $\eta^{\pm} = \sum_{z} \eta_z^{\pm}$ satisfy

$$[\mathcal{H}, \eta^{\pm}] = \pm (U - 2\mu)\eta^{\pm}, \quad [\mathcal{H}, \eta^{z}] = 0$$
 (7)

regardless of the sign of the interaction U. Exactly at half-filling, $\mu=U/2$ and all the pseudo-spin generators in equation (7) commute with $\mathcal H$ similar to the spin generators in equation (4), meaning that the Hamiltonian is invariant under global rotations of the pseudo-spin.

The pseudo-spin on a site can be visualized on the Bloch sphere like a regular spin. If it points up (down) the site contains a doublon (hole), while if it lies in the equatorial plane, the site contains an equal superposition of a doublon and hole with a complex relative phase determined by the azimuthal angle. In the limit of large attractive interactions, the spin-balanced Hubbard Hamiltonian can be approximated as a Heisenberg Hamiltonian with antiferromagnetic interactions between the pseudo-spins, leading to charge-density-wave and pairing correlations

NATURE PHYSICS DOI: 10.1038/NPHYS4297 ARTICLES

corresponding to z and x, y antiferromagnetic pseudo-spin correlations, respectively. At half-filling, the pseudo-spin rotational symmetry implies

$$\left\langle \eta_{\mathbf{r}}^{z} \eta_{\mathbf{r}+\mathbf{a}}^{z} \right\rangle_{c} = \left\langle \eta_{\mathbf{r}}^{x} \eta_{\mathbf{r}+\mathbf{a}}^{x} \right\rangle_{c} \tag{8}$$

where $\eta_{\rm r}^{\rm x} = (\eta_{\rm r}^+ + \eta_{\rm r}^-)/2$. Defining the *s*-wave pairing operator in the *x* direction as

$$\Delta_{\mathbf{r}}^{x} = c_{\mathbf{r},\uparrow} c_{\mathbf{r},\downarrow} + c_{\mathbf{r},\downarrow}^{\dagger} c_{\mathbf{r},\uparrow}^{\dagger} \tag{9}$$

one concludes that the density correlations $C^n(\mathbf{a}) = \langle n_r n_{r+\mathbf{a}} \rangle_c = 4 \langle \eta_r^z \eta_{r+\mathbf{a}}^z \rangle_c$ and pairing correlations $C^\Delta(\mathbf{a}) = \langle \Delta_r^x \Delta_{r+\mathbf{a}}^x \rangle_c = 4 \langle \eta_r^x \eta_{r+\mathbf{a}}^x \rangle_c$ are equal in magnitude at half-filling.

Deviation from half-filling introduces an effective Zeeman field along z that couples to the pseudo-spin. This leads to canted antiferromagnetic pseudo-spin correlations, with stronger correlations in the direction orthogonal to the field—that is, the pairing correlations become stronger than the density correlations. Therefore, measurement of charge-density-wave density correlations in the attractive Hubbard model provides a lower bound on the pairing correlations at any filling. In our experiment we measure a more accessible quantity, the doublon density correlator C^d (a) = $4 \langle n_i^d n_{r+a}^d \rangle_c$. The doublon density and total density correlators become equal in the limit of low temperatures and large interactions. However, the doublon density correlator C^d still provides a bound on the pairing correlator C^Δ , as we have verified numerically for the entire range of interactions, temperatures and fillings studied in the experiment (Supplementary Fig. 2).

Determinantal Quantum Monte Carlo calculations. The DQMC simulations shown in the paper were all performed using a Fortran 90/95 package called QUantum Electron Simulation Toolbox (QUEST) developed and maintained by R. T. Scalettar and colleagues⁴². For a spin-balanced system with attractive interactions (U/t < 0) the calculations do not suffer from a fermion sign problem.

Simulations for Figs 2 and 3 of the main text were performed on a square lattice of 8×8 sites with U/t = -5.7 and a chemical potential (μ/t) varying from -3 to

1.5, with $\mu=0$ representing half-filling. The inverse temperature $\beta=Ld\tau$ was split into L=40 imaginary time slices, with an interval $d\tau=0.0556$. To obtain higher statistics, the simulations were averaged over ten runs, 50,000 passes each. For Fig. 4 of the main text, U/t was fixed at -5.7 and μ to zero. The temperature was scanned by varying $d\tau$ from 0.0046 to 0.083 for a fixed L=40 and each point was averaged over 100.000 passes.

The DQMC simulations in the paper are performed using homogeneous systems. We rely on the local density approximation (LDA) for comparison to the experiment where the density varies slowly due to the harmonic trapping potential. For data shown in Supplementary Fig. 4, the density gradient at n=1 varied from 0.07 atoms/(site)² for a depth of $4.1E_{\rm R}$ to 0.14 atoms/(site)² for a depth of $7.4E_{\rm R}$. To verify that the LDA holds for our system, we have performed DQMC simulations in the presence of a linearly varying chemical potential along one direction of the 2D Hubbard lattice to reproduce the maximal density gradients observed in the experiment. The results of this calculation showed that the LDA holds to excellent approximation for our experimental parameters. However, we note that violation of the LDA had been predicted for such a system at much lower temperatures and higher gradients 51 .

Data availability. The data that support the plots within this paper and other findings of this study are available from the corresponding author upon reasonable request.

References

- Idziaszek, Z. & Calarco, T. Two atoms in an anisotropic harmonic trap. Phys. Rev. A 71, 050701 (2005).
- Zhang, S. Pseudospin symmetry and new collective modes of the Hubbard model. *Phys. Rev. Lett.* 65, 120–122 (1990).
- Assmann, E., Chiesa, S., Batrouni, G. G., Evertz, H. G. & Scalettar, R. T. Superconductivity and charge order of confined Fermi systems. *Phys. Rev. B* 85, 014509 (2012).